



**HAL**  
open science

# Relativistic effect on two-body reaction inducing atomic displacement

Shengli Chen, David Bernard

► **To cite this version:**

Shengli Chen, David Bernard. Relativistic effect on two-body reaction inducing atomic displacement. Journal of Nuclear Materials, 2019, 522, pp.236-245. 10.1016/j.jnucmat.2019.05.020 . cea-02534706

**HAL Id: cea-02534706**

**<https://cea.hal.science/cea-02534706>**

Submitted on 30 Apr 2020

**HAL** is a multi-disciplinary open access archive for the deposit and dissemination of scientific research documents, whether they are published or not. The documents may come from teaching and research institutions in France or abroad, or from public or private research centers.

L'archive ouverte pluridisciplinaire **HAL**, est destinée au dépôt et à la diffusion de documents scientifiques de niveau recherche, publiés ou non, émanant des établissements d'enseignement et de recherche français ou étrangers, des laboratoires publics ou privés.

# Relativistic effect on two-body reaction inducing atomic displacement

Shengli Chen<sup>1,2,\*</sup> and David Bernard<sup>1</sup>

<sup>1</sup> CEA, Cadarache, DEN/DER/SPRC/LEPh, 13108 Saint Paul-les-Durance, France

<sup>2</sup> Université Grenoble Alpes, I-MEP2, 38402 Saint Martin d'Hères, France

\* Corresponding author: [shengli.chen@cea.fr](mailto:shengli.chen@cea.fr)

## Abstract

The effect of the relativistic treatment of two-body reaction kinematics on atomic recoil energy and subsequent primary damage parameters, such as damage energy and number of atomic displacements, has been studied. If the emitted particle has a mass larger than the incident particle, the ratios of relativistic quantities in comparison to the classic mechanical ones can be null and infinite due to the null recoil energies. However, the relativistic corrections on recoil energies are limited in  $[-0.6\%, 0.5\%]$  and  $[-6\%, 5\%]$  for 20 MeV and 200 MeV neutron discrete  $(n,\alpha)$  reactions of  $^{56}\text{Fe}$ . For  $(n,n')$  and  $(n,p)$  reactions of any nucleus, the relativistic corrections are about 1% on recoil energy for a 20 MeV incident neutron, while the corrections can be more than 30% (about 10% on average) for 200 MeV incident energy. The relativistic effect is less than 5% on  $(\alpha,n)$  reaction inducing recoil energy of any nucleus (and within 0.6% on atomic displacement damage for  $^{56}\text{Fe}$ ) for secondary energy lower than the incident energy of 200 MeV. On the other hand, about 10 keV and 1500 keV broader Primary Knock-on Atom (PKA) spectra are respectively found for 20 MeV and 200 MeV neutron-induced  $(n,n')$ ,  $(n,p)$ , and  $(n,\alpha)$  reactions of  $^{56}\text{Fe}$ . Therefore, the relativistic treatment of two-body reactions should be applied for computing PKA spectra and subsequent radiation damage for high energy neutrons.

**Keywords:** Relativistic effect, Two-body reaction, Atomic displacement damage, Recoil energy, Damage energy

## 1. Introduction

Many physical properties of materials are changed after their irradiation by an energetic particle bombardment. The Single Event Effect (SEE) is an example of the change of physical properties under irradiation. Extensive studies on irradiation damage have been carried out over the past decades. The stable crystallographic defects in materials are formed after displacement cascades induced by the Primary Knock-on Atom (PKA). Many models have been developed to calculate the number of Displacements per Atom (DPA), which is proposed to quantify the primary radiation

damage.

Thanks to the development of computation capacity, Molecular Dynamics (MD) can calculate the DPA in crystalline using interatomic potentials. Examples of MD simulations on semiconductor and metals can be found in Ref. [1]. MD simulation allows us to compute irradiation damage for all types of materials, including polyatomic materials such as pyrochlore  $\text{La}_2\text{Zr}_2\text{O}_7$  [2]. However, MD simulations are difficult in the case of high PKA energy owing to the huge computational cost. To overcome this drawback, the Cell Molecular Dynamics for Cascades (CMDC) [3] code has been developed to accelerate the MD simulations by treating only the “active box” rather than the whole domain of the simulation. Ortiz proposed another solution that uses the MD at low energy and the Binary Collision Approximation (BCA) [4] at high energy [5].

On the other hand, some universal DPA metrics have been developed including the prototype Kinchin-Pease (KP)-DPA model [6], the current international standard Norgett-Robinson-Torrens (NRT) formula [7] and the recently proposed Athermal Recombination-Corrected (ARC) model [8]. The former two are supposed to be available for all monatomic materials, while the latter introduces MD simulation results to correct the NRT-DPA metric. Details concerning the DPA metrics are presented in Refs. [9], [10]. The NRT-DPA metric and the ARC-DPA formulae are used in the present work and briefly presented in Section 2.3.

Both MD simulation and DPA formulae use the PKA energy as a major parameter. In applications, the given quantities are the spectra of incident energetic particles, such as neutron spectra in nuclear reactors, rather than PKA spectra. For a given neutron spectrum, the corresponding PKA spectrum can be calculated by the standard code, SPECTER [11] and two recently developed codes DART [12] and SPECTRA-PKA [13]. SPECTER only uses the nuclear data library ENDF/B-V that was released in 1983. DART applies the formulae of classic mechanical kinematics. SPECTRA-PKA is based on NJOY [14], which also uses the classic mechanical formulae. Therefore, the relativistic effect has not been taken into account in these codes which transform the neutron spectra into PKA spectra.

However, a recent study shows the importance of relativistic correction for neutron scattering reactions with incident energy above 20 MeV [10]. Because neutron-induced charged particle emission channels are generally open at MeV energy, the effect of relativistic treatment should be studied for these reactions. In particular, it is important to study the relativistic corrections for neutron energy above MeV energy, such as 200 MeV DPA cross sections [15], higher than 50 MeV for the International Fusion Materials Irradiation Facility (IFMIF) [16], and even up to GeV energy for spallation neutron sources [17]–[19]. Therefore, the present work investigates the relativistic effect on PKA energy and DPA calculations for general two-body reactions, which include most of the reactions inducing atomic displacement.

## 2. Methods

### 2.1 Recoil energy of PKA within the relativistic assumption

Figure 1 illustrates the scheme of general two-body collision kinematics in the laboratory frame. The kinetic energies of the incident and the emission particles are respectively denoted by  $E$  and  $E'$ . The corresponding momenta are denoted by  $p$  and  $p'$ . Due to the negligible influence of thermal vibration of the target particle [20], the kinetic energy of the target is supposed to be 0. The recoil energy and momentum of the residual particle are denoted by  $E_R$  and  $p_R$ , respectively.  $m$ ,  $M$ ,  $m'$ , and  $M'$  represent the rest masses of the incident, target, emission, and residual particles in the ground state, respectively. The emission angle and the recoil angle are respectively denoted by  $\varphi$  and  $\alpha$ .

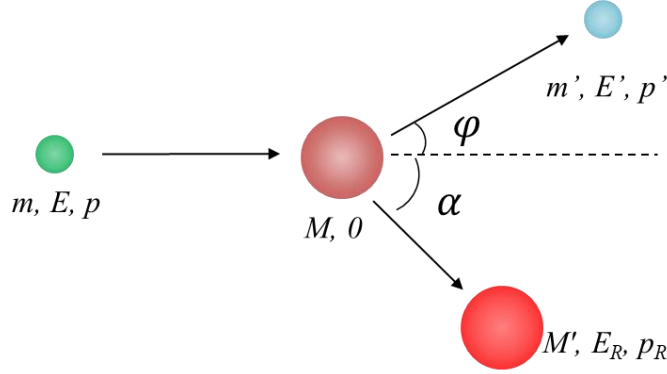


Figure 1. Scheme of the collision in a laboratory framework

The special relativity can be used in a laboratory framework that is approximatively an inertial reference. For the system illustrated in Figure 1, the conservation of momentum shows:

$$p' \sin \varphi = p_R \sin \alpha, \quad (1)$$

$$p = p' \cos \varphi + p_R \cos \alpha. \quad (2)$$

Eliminating  $\alpha$  and denoting  $\mu = \cos \varphi$ , one obtains:

$$p_R^2 = p^2 - 2pp'\mu + p'^2. \quad (3)$$

On the other hand, the relationship between relativistic momentum and energy shows:

$$p^2 c^2 + m^2 c^4 = (E + mc^2)^2, \quad (4)$$

$$p'^2 c^2 + m'^2 c^4 = (E' + m'c^2)^2, \quad (5)$$

$$p_R^2 c^2 + M'^2 c^4 = (E_R + M'c^2)^2. \quad (6)$$

For the sake of convenience, the rest energy is simply noted by the corresponding rest mass in the following equations. Replacing momenta by kinetic energies, the conservation of momentum before and after the reaction leads to:

$$E_R(E_R + 2M') = E(E + 2m) + E'(E' + 2m') - 2\sqrt{EE'(E + 2m)(E' + 2m')}\mu. \quad (7)$$

Because both the recoil energy and the right-hand side of Eq. (7) are always positive, the physical solution of Eq. (7) is:

$$E_R = \sqrt{M'^2 + E(E + 2m) + E'(E' + 2m') - 2\sqrt{EE'(E + 2m)(E' + 2m')}\mu} - M'. \quad (8)$$

The first order approximation of Eq. (8) is:

$$E_R = \frac{1}{2M'} \left[ E(E + 2m) + E'(E' + 2m') - 2\sqrt{EE'(E + 2m)(E' + 2m')}\mu \right]. \quad (9)$$

The approximation of Eq. (9) is valid for  $E_R \ll M'c^2 \approx A_R$  GeV where  $A_R$  is the mass number of the recoil particle. For incident energy that  $E/m \ll 1$ , one can further obtain the recoil energy within classic mechanical assumption as:

$$E_{R,c} = \frac{1}{M'} [mE + m'E' - 2\sqrt{mm'EE'}\mu]. \quad (10)$$

According to Eqs. (9) and (10), it is noticeable that for a specific reaction type and a given  $(E', \mu)$ , the recoil energy is inversely proportional to the mass of the residual nucleus. Therefore, the 2-D plots of recoil energies for the  $^{56}\text{Fe}$  target are general for all the nuclei by a factor of the ratio of residual masses. Moreover, the ratio of relativistic recoil energy to the classic mechanical one  $E_R/E_{R,c}$  depends only on reaction type. In other words, for a specific reaction type, the 2-D plots of  $E_R/E_{R,c}$  are exactly the same for all nuclei.

Due to the conservation of energy, the allowed range of the secondary energy in Eqs. (9) and (10) is determined by the energy loss and the recoil energy. In the present work, the maximum secondary energies are taken from JEFF-3.1.1 [21] for 20 MeV incident neutron-induced continuum reactions. For 200 MeV neutron-induced reactions, roughly assuming that the recoil energy is proportional to the incident energy (which is the case for classical elastic scattering), the reasonable maximum secondary energy becomes:

$$E'_{max}(200 \text{ MeV}) = E - 10(20 - E'_{max}(20 \text{ MeV}) - Q_t) - Q_t, \quad (11)$$

where  $Q_t$  (in MeV) is the threshold energy of the continuum reaction.

For a discrete reaction having determined excitation energy  $-Q'$  (by convention,  $Q'$  represents the increase in kinetic energy of the system due to excitation of nuclei), the conservation of energy before and after the reaction implies:

$$E' = E + Q - E_R, \quad (12)$$

where

$$Q = Q' + [m + M - (m' + M')]. \quad (13)$$

An equation governing  $E_R$  can be determined by inserting Eq. (12) into Eq. (9). Due to the square root term in Eq. (9), one puts the square root term in one side and then takes the square to eliminate the square root for solving  $E_R$ . Because the equation involving  $E_R$  is a quartic equation, numerical methods are more feasible for a determined reaction  $Q$ -value.

For a specific  $Q$ -value at given incident energy, the relationship between  $E_R$  and  $E'$  given in Eq. (12) does not depend on reaction type nor on masses of particles. On the other hand, Eq. (9) points out that  $E_R$  strongly depends on the residual mass. Therefore, the recoil energy calculated by combining Eqs. (9) and (12) with a selected  $Q$ -value and a selected target nucleus is not as general as the 2-D plots of  $E_R(E', \mu)$ , which are representative of the corresponding reaction types by a factor of the ratio of residual masses (except that the maximum secondary energy depends on nucleus).

## 2.2 Damage energy

From PKA kinetic energy to the primary radiation damage, one should consider the energy lost to the electronic excitation and ionization during the cascade of atomic collisions. The available energy to displace atoms is defined as damage energy. To compute the damage energy, Lindhard proposed integral equations governing radiation effects [22]. Using the Thomas-Fermi interatomic potential [23], [24]-based atomic collision cross sections [25], a universal partition function  $P$  that defines the fraction of PKA energy used to displace atoms is obtained for monatomic materials as [22]:

$$P(\varepsilon) = \frac{1}{1+k_L g(\varepsilon)}, \quad (14)$$

where  $\varepsilon = E_{PKA}/E_L$ , and

$$E_L = 30.724 Z_R Z (Z_R^{2/3} + Z^{2/3})^{1/2} (A_R + A)/A, \quad (15)$$

$$k_L = \frac{0.0793 Z_R^{1/3} Z^{1/2} (A_R + A)^{3/2}}{(Z_R^{2/3} + Z^{2/3})^{4/3} A_R^{3/2} A^{1/2}}, \quad (16)$$

where  $Z$  and  $A$  ( $Z_R$  and  $A_R$  resp.) are respectively the atomic number and the atomic mass number of the lattice atom (PKA resp.).  $g(\varepsilon)$  is numerically computed by Lindhard [22] and fitted by Robinson [26]:

$$g(\varepsilon) = 3.4008\varepsilon^{1/6} + 0.40244\varepsilon^{3/4} + \varepsilon. \quad (17)$$

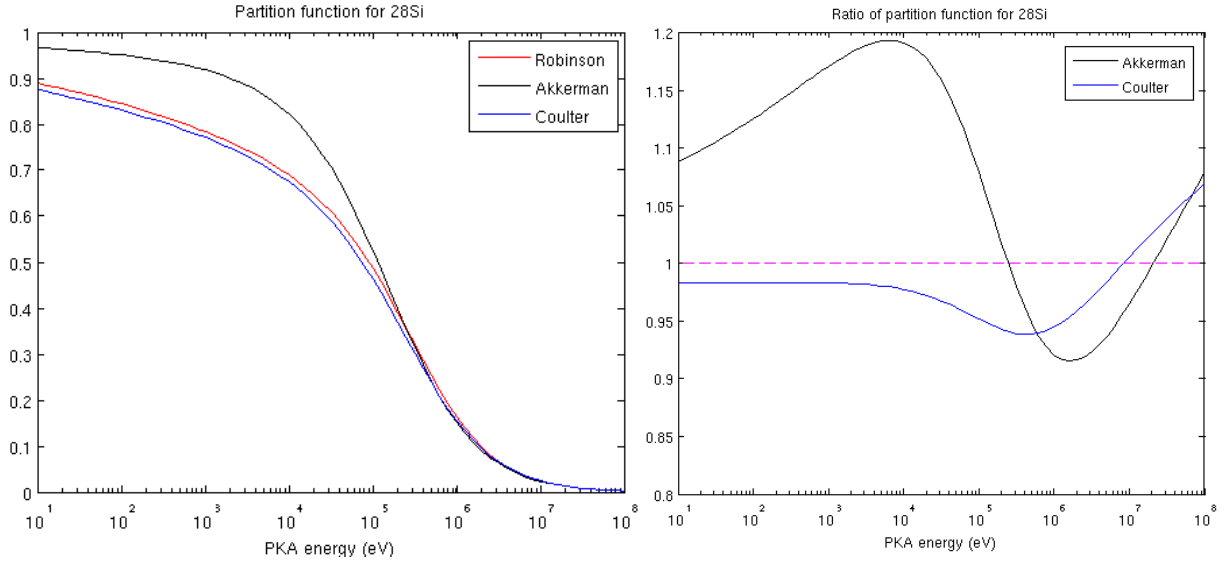


Figure 2. Different partition functions for  $^{28}\text{Si}$  (left) and the corresponding ratios to Robinson's analytic fitting (right)

Lindhard's results or Robinson's partition function are available for all isotopes. However, Akkerman and Barak found a  $g(\varepsilon)$  expression different from Robinson's formula for silicon by using the BCA [27]:

$$g(\varepsilon) = 0.90565\varepsilon^{1/6} + 1.6812\varepsilon^{3/4} + 0.74422\varepsilon. \quad (18)$$

Moreover, Coulter and Parkin [28] recalculated the partition function for monatomic materials for  $k_L$  values of 0.12, 0.15, and 0.18 using Lindhard's integral equation. For analytical expression of the partition function, the term  $\varepsilon^{1/6}$  in Robinson's function was replaced by  $\varepsilon^{0.15}$ . The average  $g$  function for  $0.12 \leq k_L \leq 0.18$  and  $0 \leq \varepsilon \leq 5000$  obtained by Coulter and Parkin is [28]:

$$g(\varepsilon) = 3.3967\varepsilon^{0.15} + 0.9863\varepsilon^{0.75} + 0.8490\varepsilon. \quad (19)$$

Although the analytical expression of Coulter is very different from that of Robinson, their results have only small differences (as illustrated in Figure 2). It is noticeable that the upper limit of Lindhard's theory [22] is  $24.9A_R Z_R^{4/3}$  keV, which is 107 MeV for  $^{56}\text{Fe}$  and 23.5 MeV for  $^{28}\text{Si}$  PKAs.

### 2.3 DPA formulae

Different DPA formulae are discussed in Ref. [9]. For the sake of convenience, this section briefly shows the two formulae used in the present work, the current international standard NRT-DPA and the MD based ARC-DPA formulae. Based on KP-DPA formula [6] and Lindhard's damage energy [22], the standard NRT-DPA [7] is expressed by:

$$N(E_a) = \begin{cases} 0, & E_a < E_d \\ 1, & E_d < E_a < 2E_d/0.8 \\ \frac{0.8E_a}{2E_d}, & E_a > 2E_d/0.8 \end{cases} \quad (20)$$

where  $E_a$  is the damage energy,  $E_d$  is the average displacement threshold energy. The widely used value of  $E_d$  is 40 eV for iron [29]. It is noteworthy that a recent Density Functional Theory (DFT)-MD study gives a value of  $30 \pm 2$  eV [30].

Due to the overestimation of the NRT-DPA formula, Nordlund *et al.* [8] proposed the ARC-DPA by introducing the relative damage efficiency  $\xi$ :

$$N(E_a) = \begin{cases} 0, & E_a < E_d \\ 1, & E_d < E_a < 2E_d/0.8 \\ \frac{0.8E_a}{2E_d} \xi(E_a), & E_a > 2E_d/0.8 \end{cases} \quad (21)$$

where:

$$\xi(E_a) = (1 - c_{arc}) \times \left[ 0.8 \frac{E_a}{2E_d} \right]^{b_{arc}} + c_{arc}, \quad (22)$$

where the coefficients  $b_{arc}$  and  $c_{arc}$  need to be fitted. Ref. [8] proposes  $b_{arc} = -0.568$  and  $c_{arc} = 0.286$  for iron using  $E_d = 40$  eV.

## 3. Results and Discussion

### 3.1 Relativistic effect on recoil energy

Figure 3 and Figure 4 respectively show the recoil energy within special relativity

(in MeV) versus  $E'$  and  $\mu$  for 20 MeV and 200 MeV neutron-induced proton production reaction (n,p) and  $\alpha$  production reaction (n, $\alpha$ ). It is remarkable that the results for the (n,n') reaction are quite similar to those of the (n,p) reaction due to the quasi-identical masses of proton and neutron. Figure 5 illustrates the same results for 200 MeV  $\alpha$  induced ( $\alpha$ ,n) reaction of  $^{56}\text{Fe}$ . As explained in Section 2.1, these 2-D plots of the recoil energy are general for the corresponding reaction types by a factor of the ratio of residual masses (except that the maximum secondary energy depends on nucleus).

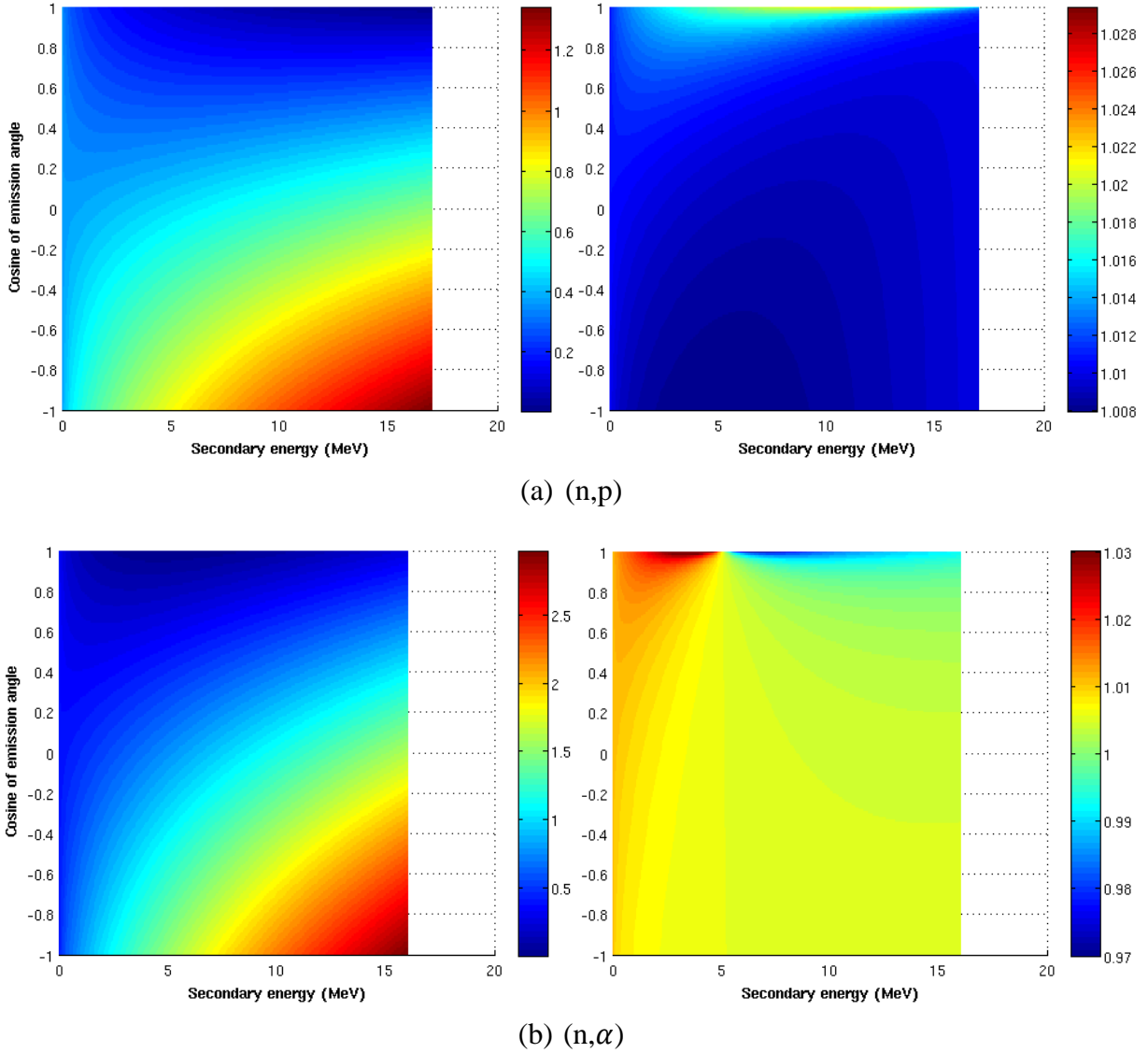


Figure 3. Recoil energy within special relativity (left, in MeV) for 20 MeV neutron-induced proton emission reaction (a) and  $\alpha$  emission reaction (b) of  $^{56}\text{Fe}$  and the ratio of relativistic to classic mechanical results for all nuclei (right)

As shown in Figure 3 and Figure 4, the global maximum (minimum resp.) recoil energies are always at  $\mu = -1$  ( $\mu = 1$  resp.) because Eq. (9) points out the decrease of  $E_R$  with  $\mu$ . For  $\mu = -1$ ,  $E_R$  increases with  $E'$ , so that the global maxima are at  $E' = E'_{max}$ . In fact, according to Eq. (9),  $E_R$  increases with  $E'$  when  $\mu \leq 0$ . For a given  $\mu > 0$ ,  $E_R$  is not a monotone function of  $E'$ . An example of a 200 MeV

neutron-induced  $(n,\alpha)$  reaction with  $\mu = 1$  is shown in Figure 6.

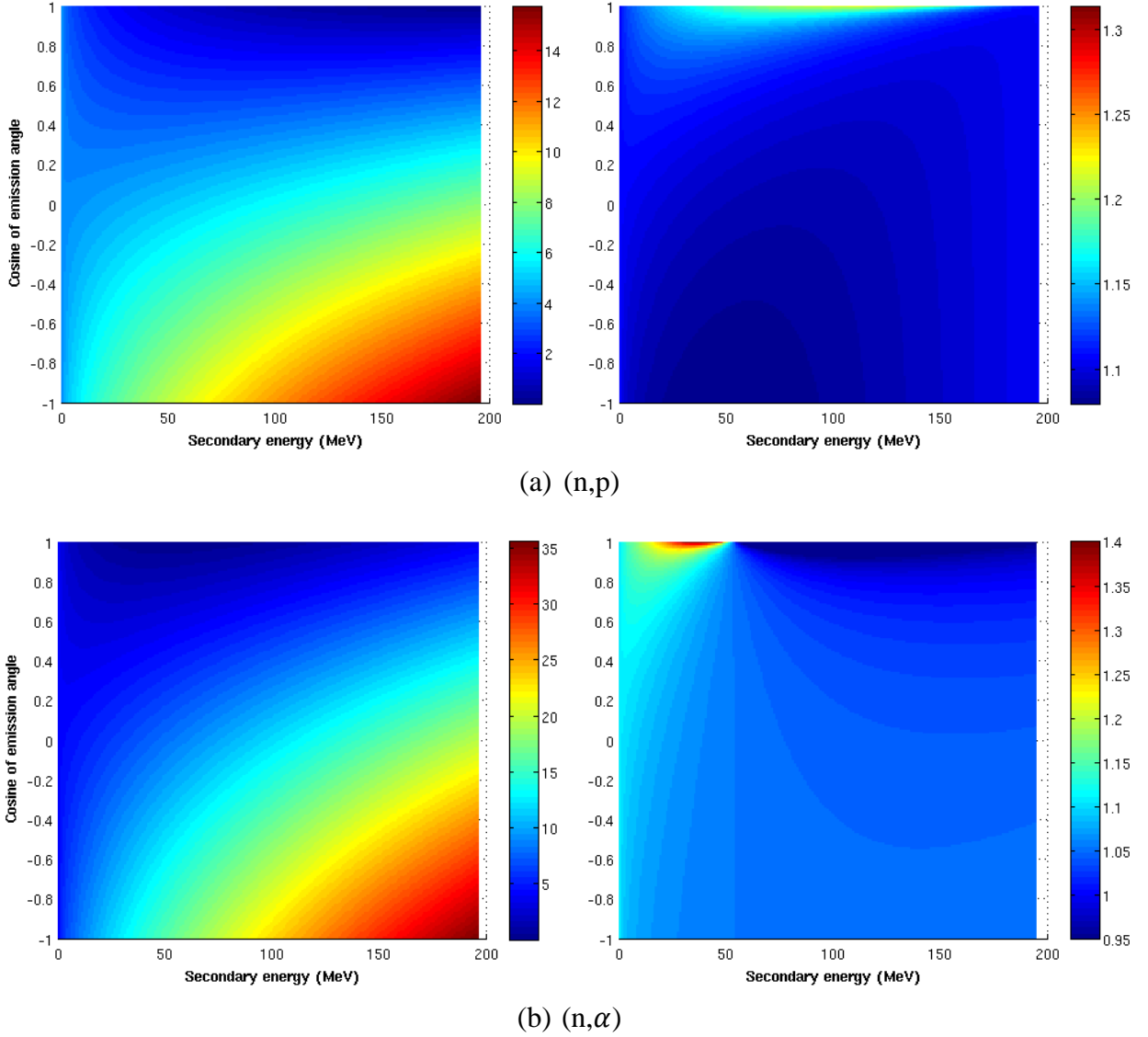


Figure 4. Recoil energy within special relativity (left, in MeV) for a 200 MeV neutron-induced proton emission reaction (a), and  $\alpha$  emission reaction (b) of  $^{56}\text{Fe}$  and the ratio of relativistic to classic mechanical results for all nuclei (right)

The corresponding ratios of recoil energies with relativistic calculations to the classic mechanical ones  $E_R/E_{R,c}$  are illustrated in the corresponding right figures of Figure 3, Figure 4 and Figure 5. Since  $E_R/E_{R,c}$  is neither independent on target particles nor recoil particles, the 2-D plots of  $E_R/E_{R,c}$  are the same for the corresponding reactions of all nuclei (except that the maximum secondary energy depends on nucleus). For the  $(n,n')$  and  $(n,p)$  reactions, the relativistic corrections on recoil energy are always positive, while both positive and negative relativistic corrections are possible for  $(n,\alpha)$  and  $(\alpha,n)$  reactions. The maximum and minimum ratios for the  $(n,\alpha)$  reaction are respectively infinite and null.

As a matter of fact, as the example shown in Figure 6, the recoil energy at  $\mu = 1$  is null at  $E' = mE/m'$  for classic mechanical collision and at  $E' =$

$\sqrt{E(E + 2m) + m'^2} - m'$  (larger than  $mE/m'$  because  $E(E + 2m) + m'^2 = (mE/m' + m')^2 + [1 - (m/m')^2]E^2$  and  $m' > m$ ) for relativistic collision. Different secondary energies at which the recoil energies are null lead to the values of infinity (i.e.  $E_{R,c} = 0$ ) and zero (i.e.  $E_R = 0$ ) for the relativistic to classic mechanical ratio. For reactions such as (n,n'), (n,p), and ( $\alpha$ ,n), because  $m' \leq m$  and  $E' < E$ , the recoil energy cannot be null, such extreme values of infinity and zero are not possible. More precisely, when  $E' < m'E/m$  or  $\mu \leq 0$ , the relativistic correction is always positive.

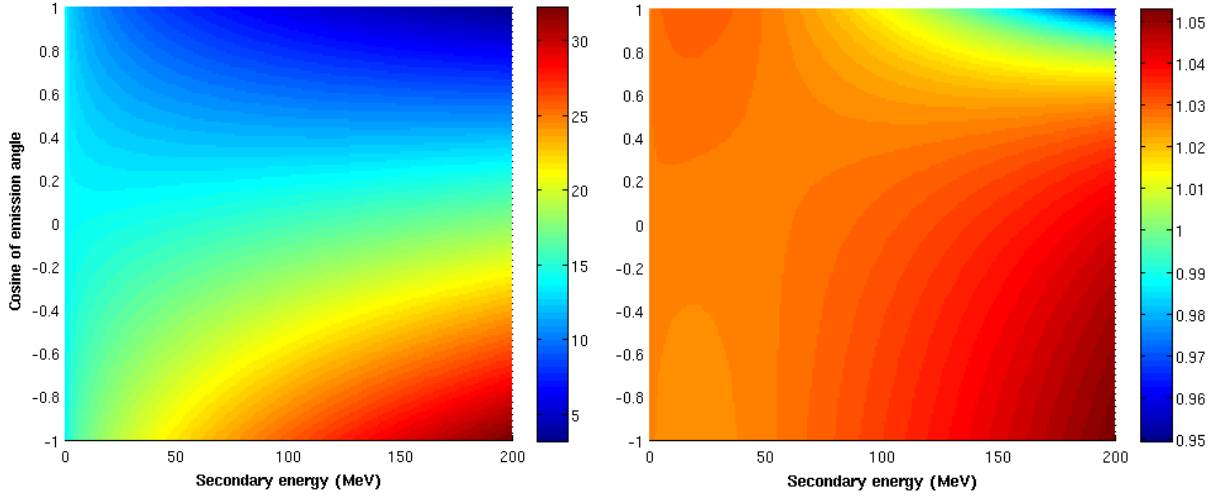


Figure 5. Recoil energy within special relativity (left, in MeV) and 200 MeV  $\alpha$  induced ( $\alpha$ ,n) reaction of  $^{56}\text{Fe}$  and the ratio of relativistic to classic mechanical results for all nuclei (right)

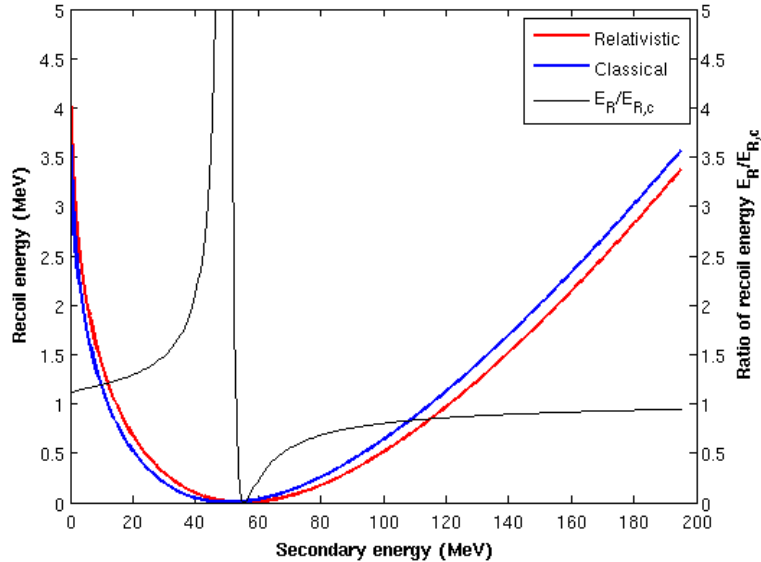


Figure 6. Recoil energies within special relativity and classical mechanics versus secondary energy for the 200 MeV neutron-induced (n, $\alpha$ ) reaction with  $^{56}\text{Fe}$  at  $\mu = 1$

For incident neutron energy below 20 MeV, the relativistic treatment has less than 3% correction on recoil energy. However, the relativistic effect should be taken into

account for high incident energy. Taking the examples of 200 MeV incident neutron, the relativistic recoil energies can be more than 30% higher than the classic mechanical ones. Moreover, large relativistic corrections on recoil energy lead to the broadening of PKA spectra. Table I gives the ranges of PKA energies for 20 MeV and 200 MeV neutron-induced (n,n'), (n,p) and (n, $\alpha$ ) reactions of  $^{56}\text{Fe}$ . The maximum recoil energy is about 10 keV and 1500 keV higher by considering the relativistic effect for 20 MeV and 200 MeV incident neutron, respectively. Such a considerable increase in maximum PKA energy implies that the range of energies for MD or BCA simulations should be extended when the relativistic effect is taken into account in PKA energy calculations.

Table I. Recoil energy ranges of 20 MeV and 200 MeV incident neutron with  $^{56}\text{Fe}$  target within classic mechanical ( $E_{R,c}$ ) and relativistic ( $E_R$ ) assumptions

$E$ (MeV)	Reaction	$E_{R,c}$ (keV)		$E_R$ (keV)	
		Min	Max	Min	Max
20	(n,n')	6.9	1250	7.1	1262
	(n,p)	2.2	1332	2.3	1345
	(n, $\alpha$ )	0.0	2955	0.0	2970
200	(n,n')	0.6	14245	0.8	15743
	(n,p)	0.4	14275	0.5	15780
	(n, $\alpha$ )	0.0	33544	0.0	35318

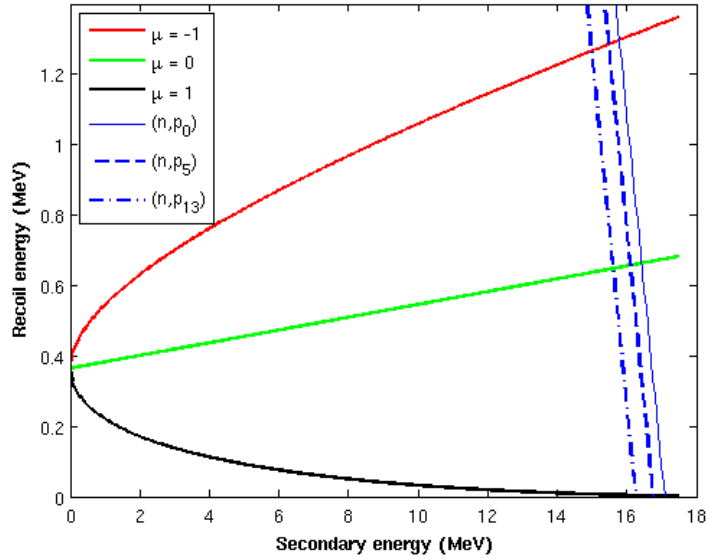


Figure 7. Recoil energy within special relativity versus secondary energy obtained with Eq. (9) ( $\mu = -1, 0, 1$ ) and Eq. (12) (blue lines) for 20 MeV neutron discrete (n,p) reactions of  $^{56}\text{Fe}$

Because the minimum PKA energies are quite smaller than the maximum ones, the ranges of PKA spectra are approximately equal to the corresponding maximum recoil energies. In addition, Eqs. (9) and (10) point out that  $E_R$  and  $E_{R,c}$  are inversely proportional to the residual mass. Consequently, for a specific reaction type at a given incident energy, the broadening of the ranges of PKA spectra due to the relativistic

effect is almost inversely proportional to the PKA mass.

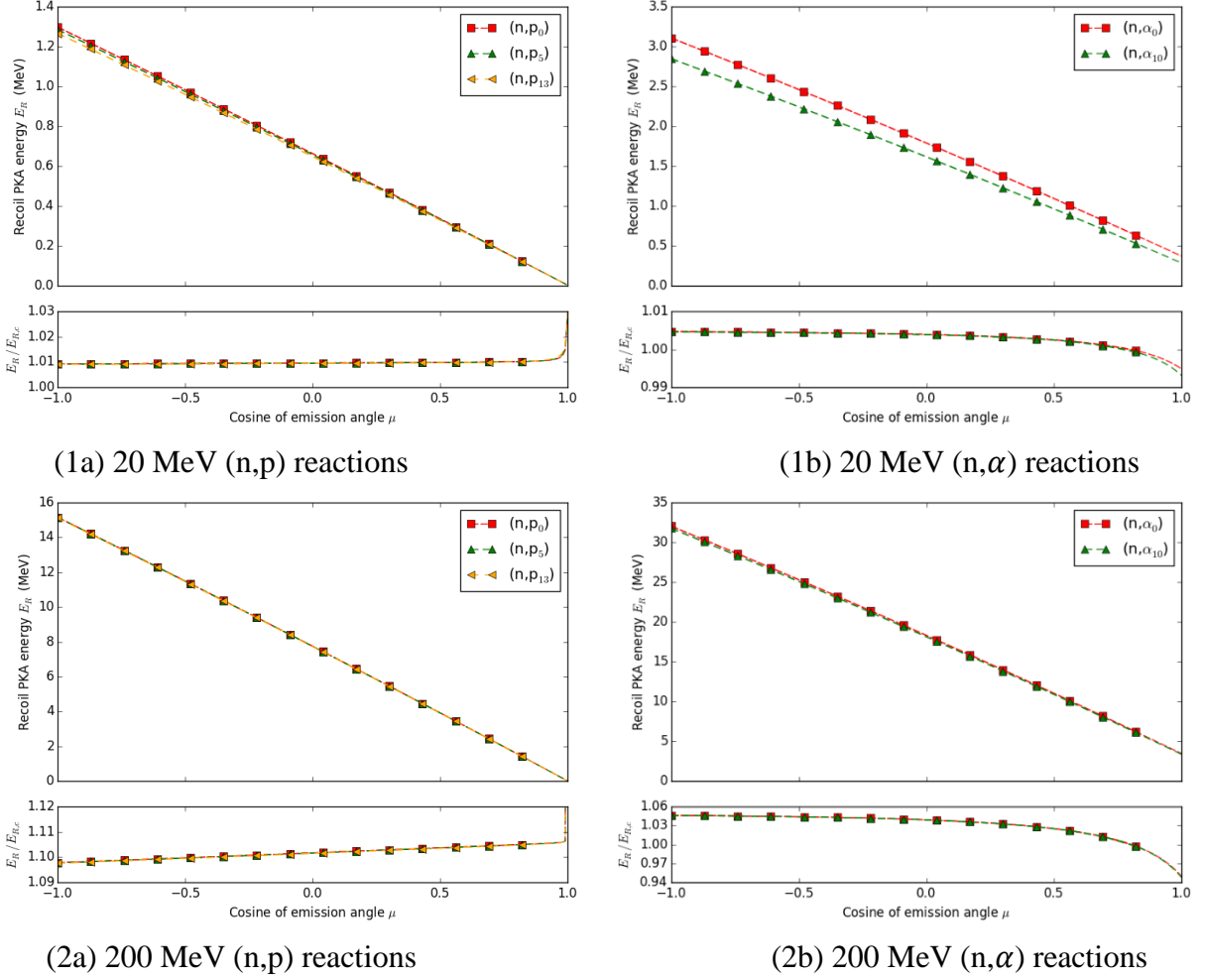


Figure 8. Recoil energy versus  $\mu$  for relativistic kinematics and the corresponding relativistic corrections for 20 MeV and 200 MeV neutron-induced discrete p and  $\alpha$  emissions of  $^{56}\text{Fe}$

For a determined reaction  $Q$ -value, the recoil energy has only one degree of freedom on  $\mu$ . Nevertheless, as mentioned in Section 2.1 the equation governing  $E_R$  is a quartic equation. Numeric method is more feasible for calculating the recoil energy. Figure 7 shows the relationship between  $E_R$  and  $E'$  according to both the conservation of momentum (i.e. Eq. (9)) and the conservation of energy (i.e. Eq. (12)) for the ground state ( $Q = -2.91$  MeV), the fifth excitation state ( $Q = -3.25$  MeV), and the thirteenth (and the last in the JEFF-3.1.1 nuclear data library [21],  $Q = -3.75$  MeV) excitation state of proton production reactions. Because the recoil energy obeys both Eq. (9) and Eq. (12), the recoil energy for a given  $\mu$  and a given  $Q$  is found at the intersection of the two corresponding curves.

The numerical results for the relativistic recoil energies of (n,p<sub>0</sub>), (n,p<sub>5</sub>), and (n,p<sub>13</sub>) reactions versus  $\mu$  and the corresponding relativistic corrections are plotted in Figure 8 for 20 MeV and 200 MeV incident neutrons. The same results for (n, $\alpha$ <sub>0</sub>) and (n, $\alpha$ <sub>10</sub>) reactions (ground state  $Q = 0.326$  MeV and the last excitation level in JEFF-3.1.1 with  $Q = -2.13$  MeV) are also shown in Figure 8. Because the recoil energies of

discrete reactions are special cases included in the general case  $E_R(\mu, E')$ , the relativistic corrections are within the range determined by Eqs. (9) and (10) and illustrated in Figure 3 and Figure 4 (probably with a higher maximum secondary energy  $E'_{max,d}$  to cover the range of  $E'$  for all discrete reactions).

The relativistic correction is almost 1% (10% resp.) for 20 MeV (200 MeV resp.) neutron-induced (n,n') and (n,p) reactions, while that of (n, $\alpha$ ) reactions is from -0.6% to 0.5% (from -6% to 5% resp.). It has been observed that for a specific discrete reaction type, the relativistic correction is not sensitive to the excitation energy. In fact, at low incident energy, the relativistic correction is quite small. At high incident energy where the relativistic correction is significant, compared with the total energy, the  $Q$ -value is negligible. Again, we notice that the relativistic corrections for discrete reactions depend on target nuclei, while the 2-D plots are representative of the corresponding reaction types by a factor of the ratio of residual masses (except that the maximum secondary energy depends on nucleus).

### 3.2 Relativistic effect on damage energy

Due to the electronic ionization and excitation, the damage energy should be studied for atomic displacement damage. Figure 10 (Figure 9 resp.) shows the relativistic damage energies and the corresponding relativistic corrections for 200 MeV neutron-induced (n,p) and (n, $\alpha$ ) reactions (200 MeV  $\alpha$  induced ( $\alpha$ ,n) reaction resp.) of  $^{56}\text{Fe}$ . Due to the small differences between different partition functions shown in Figure 2, all numerical results about the damage energy and DPA are based on Robinson's fitting [26]. Because the damage energy is an increasing function of PKA energy, the maximum and the minimum damage energies are at the same positions as recoil energies. However, due to the decrease in the partition function with PKA energy (c.f. Section 2.2 and Figure 2), the distributions of damage energy are flatter than those of recoil energy. A direct consequence is the smaller relativistic correction on damage energy than that on recoil energy.

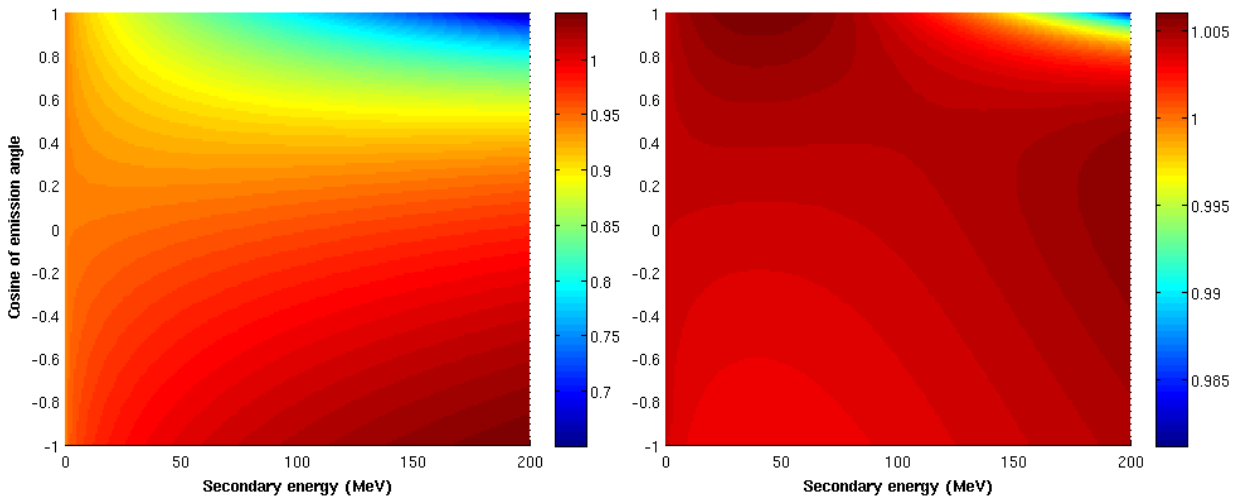


Figure 9. Damage energy within special relativity (left, in MeV) for 200 MeV  $\alpha$  induced ( $\alpha$ ,n) reaction of  $^{56}\text{Fe}$  and the corresponding ratio of relativistic to classic mechanical results (right)

For reactions where  $m'$  is evidently smaller than  $m$ , such as  $(\alpha, n)$  reaction, the minimum ratios of recoil energy  $E_R/E_{R,c}$  (as shown in Figure 5) and those of damage energy  $E_a/E_{a,c}$  (as shown in Figure 9) are at  $\mu = 1$  and  $E' = E'_{max}$ . Therefore, the precise value of  $E'_{max}$  should be determined for computing the lower boundary of relativistic correction. For secondary energy lower than the incident energy, the relativistic correction decreases with increasing mass of the incident particle (e.g. comparison between Figure 9 and Figure 10(b)).

Because the damage energy depends on the atomic number and atomic mass, the relative corrections for  $^{56}\text{Fe}$  are different to those of other isotopes. In addition, as shown in Figure 2, since the partition function depends greatly on PKA energy, for a specific PKA, same relative relativistic correction on PKA energy cannot necessarily have the same relative correction on damage energy.

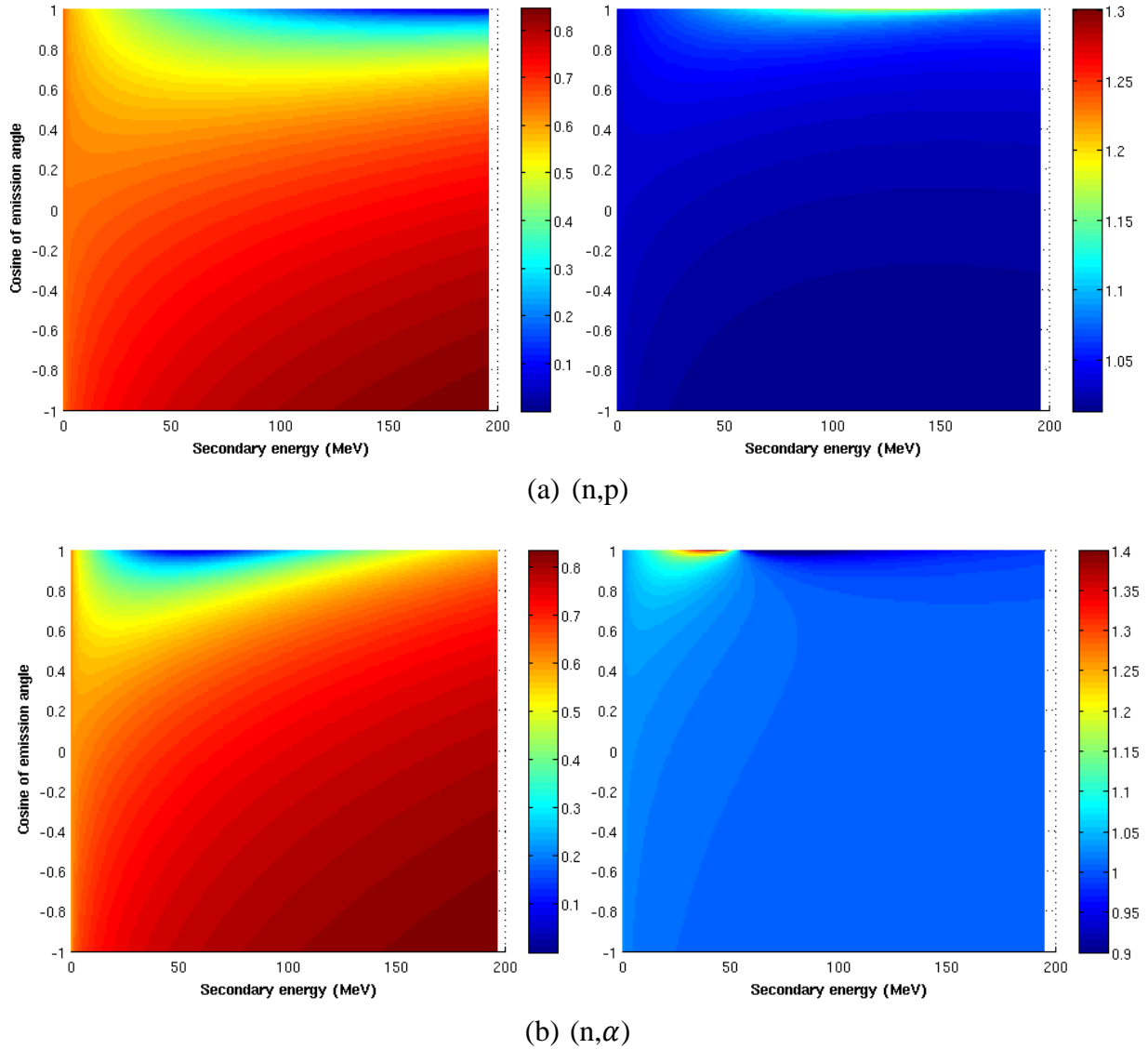
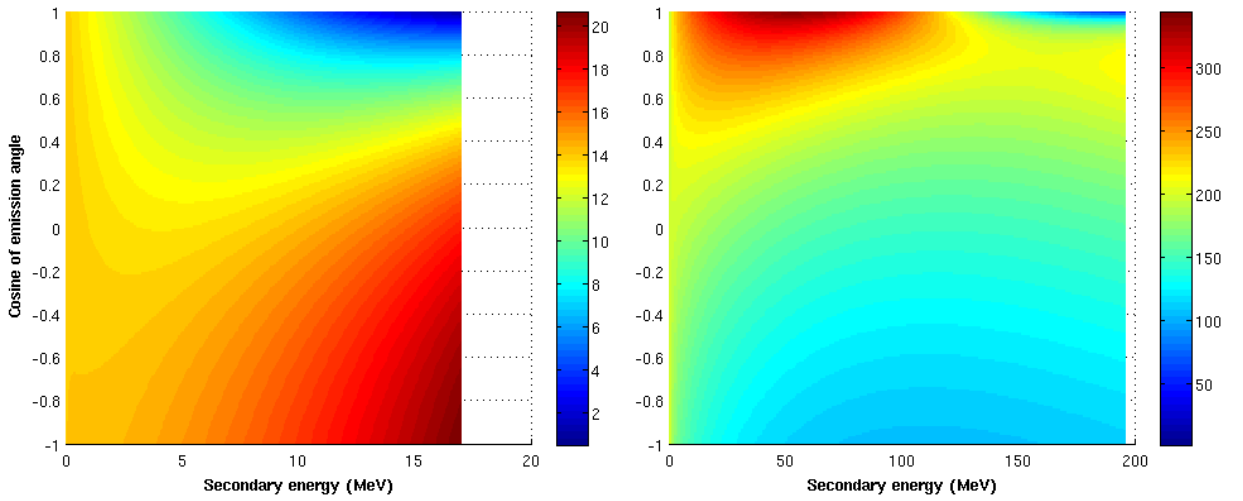


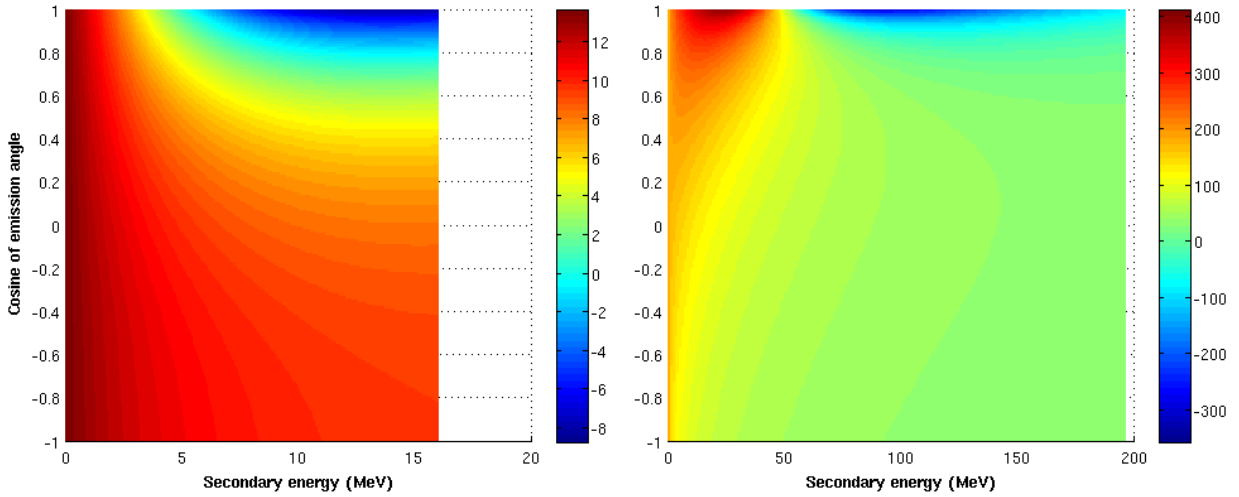
Figure 10. Damage energy within special relativity (left, in MeV) and the ratio of relativistic to classic mechanical results (right) for proton emission reaction (a) and  $\alpha$  emission reaction (b) of  $^{56}\text{Fe}$  with 200 MeV incident neutrons

### 3.3 Relativistic effect on DPA

Sections 3.1 and 3.2 point out that infinite value and zero value are possible for the ratio of relativistic PKA energy or damage energy in comparison to the classic mechanical one due to different secondary energies at which the classic mechanical and relativistic recoil energies are null. However, due to the threshold of atomic displacement, these kinds of corrections have limited influence on displacement damage. To evaluate the relativistic effect on displacement damage, the standard NRT-DPA metric [7] and the MD corrected ARC-DPA formula [8] are used.



(a) (n,p)



(b) (n,α)

Figure 11. Difference of relativistic and classic mechanical NRT-DPA for 20 MeV (left) and 200 MeV (right) incident neutrons for proton emission reaction (a) and  $\alpha$  emission reaction (b) of  $^{56}\text{Fe}$

In the NRT-DPA model, DPA is proportional to damage energy when  $E_a > 2.5E_d$ , so the 2-D plot of NRT-DPA is quite similar to that of damage energy shown in Figure

9 and Figure 10. Figure 11 (Figure 12 resp.) shows the relativistic corrections on absolute DPA number for the 20 MeV and 200 MeV neutron-induced (n,p) and (n, $\alpha$ ) reactions (200 MeV  $\alpha$  induced ( $\alpha$ ,n) reaction resp.) in terms of the NRT-DPA metric. Table II summarizes the maximum and minimum differences in DPA between relativistic and classic mechanical calculations for (n,n'), (n,p), (n, $\alpha$ ), and ( $\alpha$ ,n) reactions with 20 MeV and 200 MeV incident energies.

Table II. Maximum and minimum differences in DPA based on NRT and ARC models for  $^{56}\text{Fe}$  by introducing the relativistic effect. The relative corrections are in Table III.

$E$ (MeV)	Reaction	Max-NRT	Min-NRT	Max-ARC	Min-ARC
20 MeV	(n,n')	19.87	1.38	5.74	0.44
	(n,p)	20.65	0.50	5.96	0.17
	(n, $\alpha$ )	13.69	-8.76 <sup>b</sup>	3.97	-2.56
	( $\alpha$ ,n) <sup>a</sup>	12.98	-7.14	3.74	-2.07
200 MeV	(n,n')	350.9	1.48	101.4	0.60
	(n,p)	344.2	0.99	99.5	0.43
	(n, $\alpha$ )	413.4	-357.6	120.0	-103.9
	( $\alpha$ ,n) <sup>a</sup>	54.71	-125.0	15.74	-36.0

<sup>a</sup>  $E'_{max} = E$  is used to compute the maximum and minimum difference of DPA

<sup>b</sup> Values in italics depend on the maximum secondary energy

For (n,n') and (n,p) reactions, as the examples shown in Figure 11, the minimum differences are at  $E' = E'_{max}$ . On the other hand, Figure 10 shows that the minimum damage energies are also found at  $E' = E'_{max}$ . Because the relativistic corrections are always positive and the minima correspond to the minimum damage energies, the value of  $E'_{max}$  is not so important for evaluating the relativistic effect on damage calculations for these two reactions.

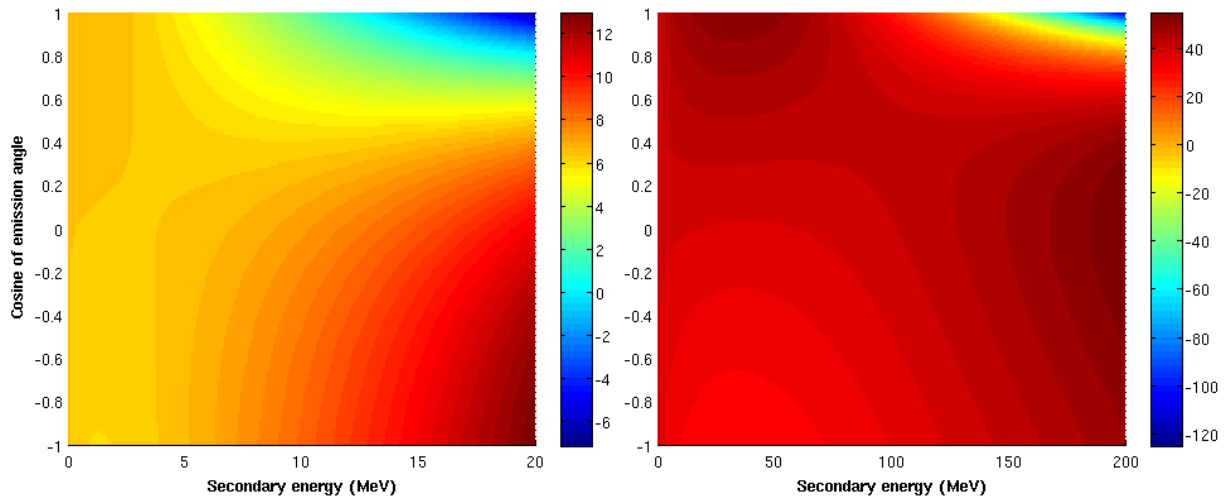


Figure 12. Difference of relativistic and classic mechanical NRT-DPA for 20 MeV (left) and 200 MeV (right)  $\alpha$  induced ( $\alpha$ ,n) reaction of  $^{56}\text{Fe}$

However, because of the negative relativistic corrections for the (n, $\alpha$ ) and ( $\alpha$ ,n)

reactions, the minimum differences are actually the maximum negative corrections for these reactions. It is the reason why the minimum differences are pointed out in Table II. Figure 11 shows that the minimum differences are found at  $E' = E'_{max}$  for the 20 MeV neutron (n, $\alpha$ ) reaction, while Figure 12 shows that the minima are at  $E' = E'_{max}$  for the ( $\alpha$ ,n) reaction with  $\alpha$  energy up to 200 MeV. Therefore, the minima in Table II in italics depends on  $E'_{max}$ . If we change the  $E'_{max}$  of continuum reactions by the maximum  $Q$ -value (i.e. without considering excitation), these values would be smaller (larger in absolute values). However, because the recoil energies of discrete reactions are strictly included in  $E_R(E', \mu)$  in the range up to  $E'_{max,d}$ , the minimum differences are lower than the real minima if  $E'_{max,d}$  is used.

The maximum relativistic corrections are quite close for (n,n') and (n,p) reactions because of the very close masses for neutron and proton ( $m_p/m_n = 0.99917$ ) and  $^{56}\text{Fe}$  and  $^{56}\text{Mn}$  ( $m_{^{56}\text{Mn}}/m_{^{56}\text{Fe}} = 1.00008$ ). The relativistic effect on the number of DPA is smaller for the (n, $\alpha$ ) reaction than (n,n') and (n,p) reactions for 20 MeV neutrons, but larger for 200 MeV neutrons. Due to the much larger mass of  $\alpha$  than that of neutron, the relativistic correction of ( $\alpha$ ,n) reaction induced DPA number is quite smaller than that of the neutron-induced reaction, especially for 200 MeV incident energy.

### 3.4 Summary of relativistic corrections

To globally evaluate the relativistic effect on atomic displacement, Table III summarizes the maximum ratios of relativistic quantities to the classic mechanical ones for recoil energy, damage energy, and the NRT metric-based DPA number. It is noticeable that the ratios of NRT-DPA given in Table III are exactly the same as the ratios based on ARC-DPA because the high PKA energies lead to the constant efficiency  $\xi = c_{arc}$ . As explained in Section 3.1, the infinity for recoil energy and damage energy of the (n, $\alpha$ ) reaction is due to the null classic mechanical recoil energy. As for DPA, if there is one point at which the classic mechanical damage energy is below the threshold energy while the relativistic one is above, the ratio is infinite.

Table III. Maximum ratio of relativistic quantities to the classical ones

$E$ (MeV)	Reaction	Recoil energy	Damage energy <sup>b</sup>	NRT-DPA <sup>b</sup>
20 MeV	(n,n')	1.028	1.027	1.027
	(n,p)	1.029	1.028	1.028
	(n, $\alpha$ )	$\infty$	$\infty$	$\infty$
	( $\alpha$ ,n) <sup>a</sup>	1.005	1.002	1.002
200 MeV	(n,n')	1.325	1.314	1.314
	(n,p)	1.314	1.301	1.301
	(n, $\alpha$ )	$\infty$	$\infty$	$\infty$
	( $\alpha$ ,n) <sup>a</sup>	1.053	1.006	1.006

<sup>a</sup>  $E'_{max} = E$  is used to compute the maximum and minimum difference of DPA

<sup>b</sup> For  $^{56}\text{Fe}$  target

For incident neutron energy lower than 20 MeV, the relativistic corrections are

within 3%. Except for the small region in which the relativistic effect is obviously more important than other regions (e.g. Figure 3), the relativistic corrections are about 1% in the damage calculation for the (n,n') and (n,p) reactions. For 200 MeV neutron, the maximum corrections are more than 30% (and about 10% on average). Consequently, the computation of PKA spectra and damage cross sections for neutron energy up to 200 MeV (and higher for spallation neutron sources) should be based on the relativistic kinematics.

For a given incident energy, the relativistic effect is less important for incident particles with higher masses. As summarized in Table III, the maximum relativistic correction of 200 MeV  $\alpha$ -induced neutron emission reaction is only 5% on PKA energy and lower on damage energy. In contrast, the relativistic effect is always taken into account for electron, positron and photon-induced damage calculations [31].

## 4. Conclusions

The relativistic effect is not considered in traditional codes for PKA energy calculations with an external incident particle. The present work investigates the relativistic effect for general two-body reaction kinematics. The relativistic effect is further examined in atomic displacement damage calculations using the damage energy and two DPA formulae. For reactions where the mass of the emitted particle  $m'$  is different to that of incident particle  $m$ , both positive and negative relativistic corrections are possible on recoil energy as on atomic displacement damage. For  $m' > m$ , due to the possible null recoil energy, the ratios of relativistic quantities, including recoil energy, damage energy, and DPA, in comparison to the classic mechanical ones can be infinite and null. For  $m' = m$ , the relativistic correction is always positive.

For a given incident energy, because the relativistic effect decreases with mass, the relativistic correction is generally less for heavier incident particles. For example, the relativistic correction on PKA energy is less than 5% for 200 MeV  $\alpha$ -induced ( $\alpha$ ,n) reaction with secondary energy lower than incident energy, while that of the 200 MeV neutron-induced (n,n'), (n,p) and (n, $\alpha$ ) reactions can be higher than 30%. In the case of  $^{56}\text{Fe}$  target, the relativistic corrections are within 0.6% for the 200 MeV ( $\alpha$ ,n) reaction.

The relativistic corrections are about 1% (the maximum is within 3%) for 20 MeV neutron-induced scattering and proton production reactions. However, the relativistic corrections can be more than 30% (about 10% on average) higher than the classic mechanical ones for 200 MeV neutron-induced (n,n') and (n,p) reactions. For discrete (n,n') and (n,p) reactions of  $^{56}\text{Fe}$ , the relativistic corrections are respectively 1% and 10% for 20 MeV and 200 MeV incident energy. Although the relativistic corrections can be null and infinite for the continuum (n, $\alpha$ ) reaction, the corresponding corrections on PKA energies range from -0.6% to 0.5% (from -6% to 5% resp.) for 20 MeV (200 MeV resp.) neutron-induced discrete (n, $\alpha$ ) reactions of  $^{56}\text{Fe}$  target.

In comparison with classic mechanical kinematical calculations, the broadening of the PKA spectra for a specific reaction at a given incident energy is quasi-inversely proportional to the PKA mass. For  $^{56}\text{Fe}$  target, about 10 keV (1500 keV resp.) broader PKA energy is found for 20 MeV (200 MeV resp.) neutron-induced reactions by

considering the relativistic effect. Consequently, the range of PKA energies for damage calculations should be extended. In addition, for incident neutron energy above several tens MeV, which is the case for the IFMIF [16] and spallation neutron sources, the relativistic effect should be taken into account for atomic displacement damage calculations.

## References

- [1] K. Nordlund, M. Ghaly, R. S. Averback, M. Caturla, T. Diaz de la Rubia, and J. Tarus, “Defect production in collision cascades in elemental semiconductors and fcc metals,” *Phys. Rev. B*, vol. 57, no. 13, pp. 7556–7570, Apr. 1998.
- [2] A. Chartier, C. Meis, J.-P. Crocombette, L. R. Corrales, and W. J. Weber, “Atomistic modeling of displacement cascades in  $\text{La}_2\text{Zr}_2\text{O}_7$  pyrochlore,” *Phys. Rev. B*, vol. 67, no. 17, p. 174102, May 2003.
- [3] J.-P. Crocombette and T. Jourdan, “Cell Molecular Dynamics for Cascades (CMDC): A new tool for cascade simulation,” *Nucl. Instrum. Methods Phys. Res. Sect. B Beam Interact. Mater. At.*, vol. 352, pp. 9–13, Jun. 2015.
- [4] M. T. Robinson and I. M. Torrens, “Computer simulation of atomic-displacement cascades in solids in the binary-collision approximation,” *Phys. Rev. B*, vol. 9, no. 12, pp. 5008–5024, Jun. 1974.
- [5] C. J. Ortiz, “A combined BCA-MD method with adaptive volume to simulate high-energy atomic-collision cascades in solids under irradiation,” *Comput. Mater. Sci.*, vol. 154, pp. 325–334, Nov. 2018.
- [6] G. H. Kinchin and R. S. Pease, “The Displacement of Atoms in Solids by Radiation,” *Rep Prog Phys*, vol. 18, no. 1, pp. 1–51, 1955.
- [7] M. J. Norgett, M. T. Robinson, and I. M. Torrens, “A proposed method of calculating displacement dose rates,” *Nucl. Eng. Des.*, vol. 33, no. 1, pp. 50–54, 1975.
- [8] K. Nordlund *et al.*, “Improving atomic displacement and replacement calculations with physically realistic damage models,” *Nat. Commun.*, vol. 9, no. 1, 2018.
- [9] K. Nordlund, A. E. Sand, F. Granberg, S. J. Zinkle, and R. E. Stoller, “Primary Radiation Damage in Materials,” OECD/NEA Working Party on Multiscale Modelling of Fuels and Structural Materials for Nuclear Systems, Expert Group on Primary Radiation Damage Nuclear Science, NEA/NSC/DOC(2015)9, 2015.
- [10] S. Chen and D. Bernard, “Application of special relativity in damage calculations,” *Nucl. Instrum. Methods Phys. Res. Sect. B Beam Interact. Mater. At.*, vol. 440, pp. 107–113, Feb. 2019.
- [11] L. R. Greenwood and R. K. Smither, “SPECTER: Neutron damage calculations for materials irradiations,” Argonne National Laboratory, Argonne National Laboratory, ANL/FPP/TM-197, Jan. 1985.
- [12] L. Lunéville, J. C. Sublet, and D. Simeone, “Impact of nuclear transmutations on the primary damage production: The example of Ni based steels,” *J. Nucl. Mater.*, vol. 505, pp. 262–266, Jul. 2018.
- [13] M. R. Gilbert, J. Marian, and J.-C. Sublet, “Energy spectra of primary knock-on

- atoms under neutron irradiation,” *J. Nucl. Mater.*, vol. 467, pp. 121–134, Dec. 2015.
- [14] R. E. MacFarlane and A. C. Kahler, “Methods for Processing ENDF/B-VII with NJOY,” *Nucl. Data Sheets*, vol. 111, no. 12, pp. 2739–2890, Dec. 2010.
- [15] A. Y. Konobeyev, U. Fischer, and S. P. Simakov, “Atomic displacement cross-sections for neutron irradiation of materials from Be to Bi calculated using the arc-dpa model,” *Nucl. Eng. Technol.*, vol. 51, no. 1, pp. 170–175, Feb. 2019.
- [16] S. P. Simakov and U. Fischer, “Displacement damage induced in iron by gammas and neutrons under irradiation in the IFMIF test cell,” *J. Nucl. Mater.*, vol. 417, no. 1–3, pp. 1321–1324, Oct. 2011.
- [17] O. A. Shcherbakov, E. M. Ivanov, G. F. Mikheev, G. A. Petrov, G. A. Riabov, and A. S. Vorobyev, “Spallation Neutron Source at the 1 GeV Synchrocyclotron of PNPI,” in *Proceedings of RuPAC2016*, St. Petersburg, Russia, 2017, pp. 90–94.
- [18] L. K. Mansur, A. F. Rowcliffe, R. K. Nanstad, S. J. Zinkle, W. R. Corwin, and R. E. Stoller, “Materials needs for fusion, Generation IV fission reactors and spallation neutron sources – similarities and differences,” *J. Nucl. Mater.*, vol. 329–333, pp. 166–172, Aug. 2004.
- [19] P. W. Lisowski, C. D. Bowman, G. J. Russell, and S. A. Wender, “The Los Alamos National Laboratory Spallation Neutron Sources,” *Nucl. Sci. Eng.*, vol. 106, no. 2, pp. 208–218, Oct. 1990.
- [20] S. Chen, D. Bernard, and L. Buiron, “Study on the self-shielding and temperature influences on the neutron irradiation damage calculations in reactors,” *Nucl. Eng. Des.*, vol. 346, pp. 85–96, May 2019.
- [21] A. Santamarina *et al.*, “The JEFF-3.1.1 Nuclear Data Library,” OECD/NEA, JEFF Report 22, NEA No. 6807, 2009.
- [22] J. Lindhard, V. Nielsen, M. Scharff, and P. V. Thomsen, “Integral equations governing radiation effects,” *Mat Fys Medd Dan Vid Selsk*, vol. 33, no. 10, pp. 1–42, 1963.
- [23] E. Fermi, “Statistical method to determine some properties of atoms,” *Rend Accad Naz Lincei*, vol. 6, no. 602–607, p. 5, 1927.
- [24] L. H. Thomas, “Calculation of Atomic Fields,” *Math. Proc. Camb. Philos. Soc.*, vol. 23, no. 5, pp. 542–548, 1927.
- [25] J. Lindhard, V. Nielsen, and M. Scharff, “Approximation Method in Classical Scattering by Screened Coulomb Fields,” *Kgl Dan Vidensk Selsk Mat-Fys Medd*, vol. 36, no. 10, pp. 1–32, 1968.
- [26] M. T. Robinson, “Energy Dependence of Neutron Radiation Damage in Solids,” *Nucl. Fusion React.*, pp. 364–378, 1970.
- [27] A. Akkerman and J. Barak, “New Partition Factor Calculations for Evaluating the Damage of Low Energy Ions in Silicon,” *IEEE Trans. Nucl. Sci.*, vol. 53, no. 6, pp. 3667–3674, Dec. 2006.
- [28] C. A. Coulter and D. M. Parkin, “Damage energy functions in polyatomic materials,” *J. Nucl. Mater.*, vol. 88, no. 2, pp. 249–260, 1980.
- [29] ASTM E693-94, *Standard Practice for Characterizing Neutron Exposures in Iron and Low Alloy Steels in Terms of Displacements Per Atom (DPA), E706(ID)*. West

Conshohocken, PA: ASTM International, 2001.

- [30] P. Olsson, C. S. Becquart, and C. Domain, “Ab initio threshold displacement energies in iron,” *Mater. Res. Lett.*, vol. 4, no. 4, pp. 219–225, Oct. 2016.
- [31] S. Chen, D. Bernard, and C. De Saint Jean, “Calculation and analysis of gamma-induced irradiation damage cross section,” *Nucl. Instrum. Methods Phys. Res. Sect. B Beam Interact. Mater. At.*, vol. 447, pp. 8–21, May 2019.